Multi-dimensional AWI: theory and application in the Eastern Mediterranean

John Reilly, Tenice Nangoo, Adrian Umpleby, Nikhil Shah, and Mike Warner, S-Cube; Henry A. Debens, James Cai, and Teresa Castro Leyva, Woodside Energy*

Summary

FWI iteratively refines subsurface velocity models by minimizing the misfit between observed and simulated datasets. AWI is a robust deconvolution-based misfit function for FWI that performs well with poor initial models and incomplete wave physics. Here we demonstrate that conventional 1D AWI can be extended to higher dimensions: 2D AWI for towed-streamer data and 3D AWI for ocean-bottom data. These extensions are particularly effective for datasets that show significant elastic effects. For a marine towed-streamer dataset exhibiting moderate elastic behavior, combining 1D and 2D AWI enabled accurate kinematic matching, and captured steep velocity features likely to be associated with zones of enhanced simple shear, while avoiding overfitting finer details. The resulting AWI model produced simpler structures following Kirchhoff pre-stack depth migration, and produced significantly flatter gathers, when compared to a workflow that combined reflection tomography and conventional FWI.

Introduction

Full-waveform inversion (FWI) typically builds subsurface velocity models by iteratively updating an initial model to minimize some measure of misfit between an observed field dataset and an equivalent numerically simulated predicted dataset. The simplest measure of misfit commonly used is the sum of the squares of the sample-by-sample differences between the two datasets. This measure works well provided the initial model is close to the true answer, and the simulation is a good match to the true physics of the wavefield propagation. More advanced misfit functions help to relax these requirements.

One such family of misfit functions is known collectively as adaptive waveform inversion or AWI (Warner and Guasch, 2016; Guasch et al., 2019). Rather than subtracting one dataset from another, and attempting to drive the resulting differences to zero, AWI instead deconvolves one dataset from the other, and attempts to drive the result of that deconvolution to unity. More precisely, AWI derives a suite of convolutional filters that match one dataset to the other, and it sets up a misfit function that acts to drive those filters towards zero-lag, band-limited, delta functions as the two datasets become more alike. Typically, AWI filters are 1D, and they act trace by trace, matching one entire trace to the other. Here we demonstrate that multi-dimensional AWI filters, acting over both space and time, matching an entire shot record to another, can be employed advantageously for datasets that show significant elastic effects.

Method

Figure 1 illustrates the principle of 2D AWI for a conventional narrow-azimuth multi-streamer marine field dataset. The left panels show observed and predicted low-pass filtered single-source/single-streamer shot records. The upper-right panel shows the suite of band-limited 1D convolutional filters required to match the observed to the predicted data, trace by trace. The lower-right panel shows the analogous 2D filter designed to match the entire shot record. The AWI misfit function used in 1D AWI is designed to update the model so that its filters each collapse towards zero temporal lag. In contrast, the misfit function for 2D AWI is designed to collapse the single 2D filter towards zero for both temporal and spatial lag. For a perfect final model, Figure 1c will become a (band-limited) horizontal central line while Figure 1d will become a (band-limited) single central point.

Conventional 1D AWI is based partly upon the idea that model errors typically cause predicted data to arrive at incorrect times. Unlike simple least-squares FWI, it is formulated so that the initial errors in arrival times can be larger than half a cycle, such that AWI does not suffer from temporal cycle-skipping. Multi-dimensional AWI is similarly based upon the idea that model errors may cause predicted data to arrive at both the wrong time and the wrong location, and is formulated such that it can overcome both temporal and spatial cycle-skipping. We would expect therefore that multi-dimensional AWI would be better able to deal with velocity models that contain steeply dipping structure than would the simpler 1D formulation, and indeed, that is what we observe.

Practical implementations of multi-dimensional AWI typically require careful stabilization of the deconvolution, appropriate tiling in space and time, and spatial tapering to control edge effects. The approach is most straightforward to implement when receivers are uniformly spaced within a shot record along individual towed streamers, or when sources are uniformly spaced in two dimensions within a receiver record for ocean-bottom data. Experimentally, we find that 2D AWI is typically able to generate larger model updates than 1D AWI, and so can proceed using fewer iterations, but that it is also more prone to overshoot the true model than is its 1D analogue. Both methods have immunity

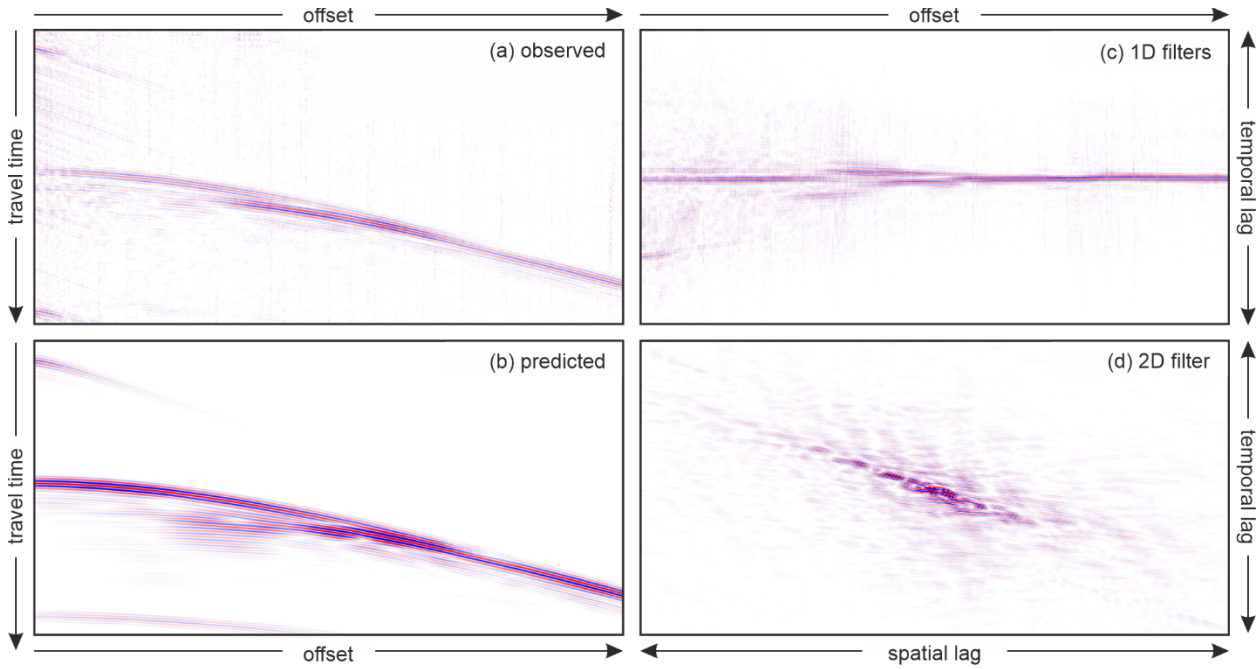

Figure 1: Shot record for a single source recorded by a single streamer: (a) observed field data, (b) predicted data, (c) the 1D filters that match the observed to the predicted data trace by trace, and (d) the 2D filter that matches the entire observed shot record to the predicted shot record.

to cycle-skipping, and both methods are better able to recover an accurate model when the physics assumed in the simulation are less complete than those displayed by the field data.

Application in the Eastern Mediterranean

We have applied a combination of 2D AWI, 1D AWI, and least-squares FWI to a narrow-azimuth towed-streamer 3D field dataset from the Eastern Mediterranean, offshore Egypt, acquired over variable water depths for exploration purposes (Figure 2). These data were acquired in 2020 using sixteen multi-component streamers, 8 km in length, and three sources; only the hydrophone data were inverted here. The sections in Figure 2 extend to 8 km depth; the Kirchhoff migrations have had no post-processing applied and used a 5–35° angle mute. The shallow-water section shows low-velocity clastics above a thick fast carbonate platform. The deeper-water section shows rapidly deepening carbonates, overlain by a thick clastic section, capped by fast, finely layered evaporites. Reflections and multiples from the top of the carbonates, the rugged dipping edge of the platform, the top of the evaporites, and, to a lesser extent, the seabed, all generate significant elastic effects in the field data.

After extensive testing of both acoustic and elastic waveform inversion, and of various formulations and combinations of 1D AWI, 2D AWI, and conventional FWI, we applied a purely acoustic scheme over the full area of interest using public-cloud compute resources, in which elastic effects were partially mitigated by AWI. We interleaved 2D and 1D AWI within each iteration block, inverting over the full range of offsets, from 3 to 10.7 Hz. The model building was completed using a pass of conventional least-squares FWI at 10.7 Hz. The underlying rationale is that 2D AWI makes rapid early progress within each new frequency range and is best able to recover steep dips. 1D AWI then acts to remove any model overshoot, and it matches the kinematics accurately despite considerable elastic effects in the raw field data. Finally, acoustic FWI helps to match the reflection dynamics.

The legacy model in Figure 2 used a combination of ray-based tomography and FWI as part of an interleaved model-building workflow. There are significant differences between the legacy and AWI velocity models over a wide range of length scales, where the average velocity is generally higher in the AWI-derived model. Comparing the migrations in Figure 2, the AWI-based result is structurally simpler, has greater bandwidth, and has a stronger stack response. The enhanced simplicity of the AWI-based migration strongly suggests that the undulations in depth seen in the legacy migration are related to unrecovered detail in the velocity model that were best captured by AWI.

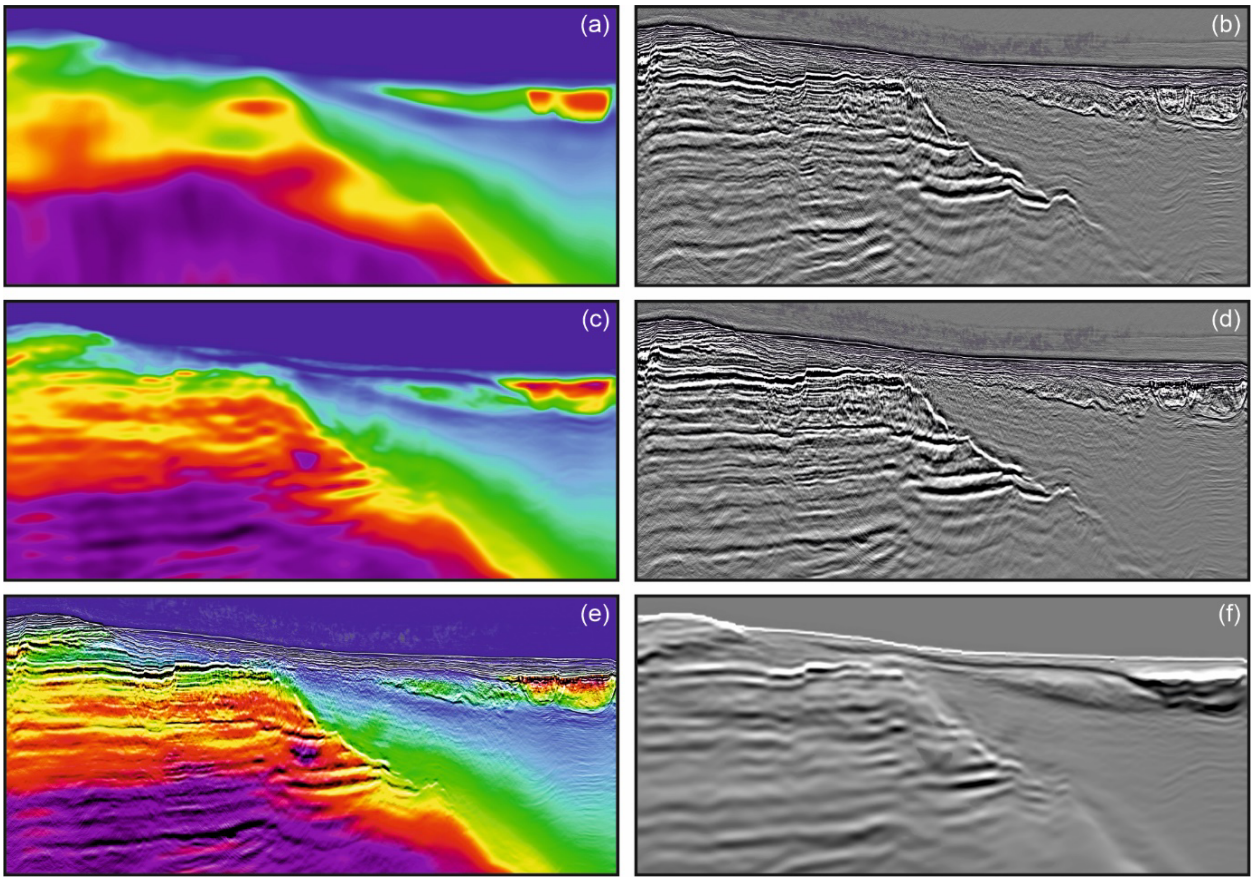

Figure 2: Velocity models and associated images. (a) Legacy model and (b) corresponding Kirchhoff-migrated depth section. (c) Final AWI model and (d) corresponding Kirchhoff migration. (e) AWI model with migration overlain. (f) Acoustic reflectivity extracted directly from the AWI model at 10.7 Hz.

Figure 3 shows raw Kirchhoff common-image gathers (CIGs) for the two models. The displayed offset range is limited to 5.5 km, and automatic gain control has been applied using a 1000 ms window. In the upper portion of the CIGs, the moveout is mostly overcorrected by the legacy model; the gathers are more consistently flat in the AWI model. At greater depths, the AWI CIGs are flatter, simpler, and better focused. There are strong low-velocity multiples still clearly present in the migrated data; it is likely therefore that both reflection tomography and conventional FWI have been misled in part by the larger moveout of those multiples, biasing the recovered velocity towards their lower velocities. Even for weakly elastic data, the amplitude-versus-angle behavior and absolute amplitude of multiples are normally less well modelled by acoustic waves than are the primary reflections. AWI's ability to capture kinematics accurately in the presence of significant event-dependent amplitude mismatch appears to have been able here to circumvent this problem. Reflectivity derived directly from the AWI model, Figure 2f, suggests no evidence of multiple contamination.

Figure 4 shows a zoomed section of an AWI model, its derived reflectivity, and the model overlain by its Kirchhoff migration; the color scale is not the same as that used in Figure 2, and the inversion here was run to a maximum frequency of 21.4 Hz. A steep left-dipping feature is seen in the recovered velocity model and in the model reflectivity. The higher-bandwidth migration shows that this feature is associated with a normal fault and an adjacent region of post-depositional distributed shear parallel to the fault.

This, and related steep features, were not seen in analogous models derived from 1D AWI or conventional FWI; they only appear on models that have used 2D AWI. Analogous features do not appear in the model for sharp, narrow faults that have little or no associated zone of distributed simple shear. It appears that 2D AWI is able to map the effects of distributed intense shear deformation, perhaps through the direct effects on velocity, through subsequent enhancement of sedimentation in those zones, or perhaps because of large, localized changes in anisotropy. Not all such steep features

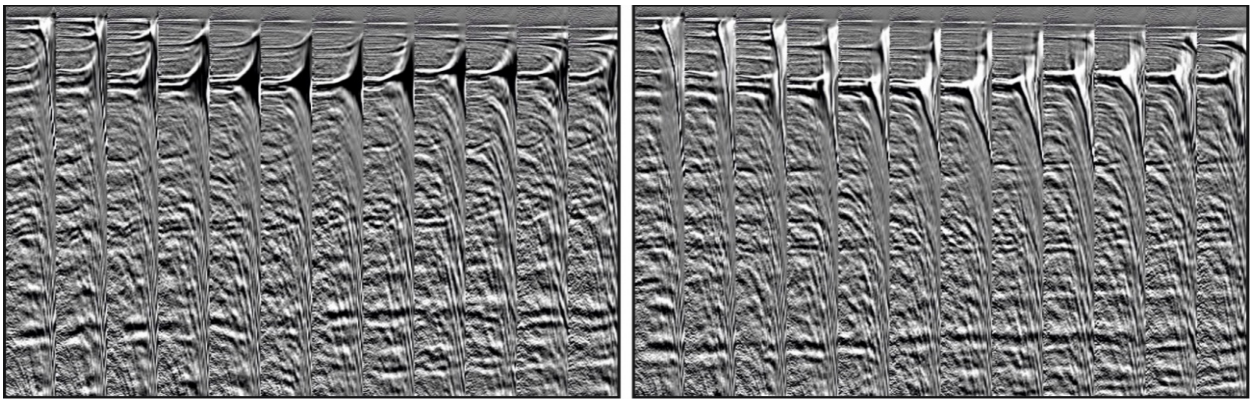

Figure 3: Raw Kirchhoff CIGs: legacy model (left) and final model (right).

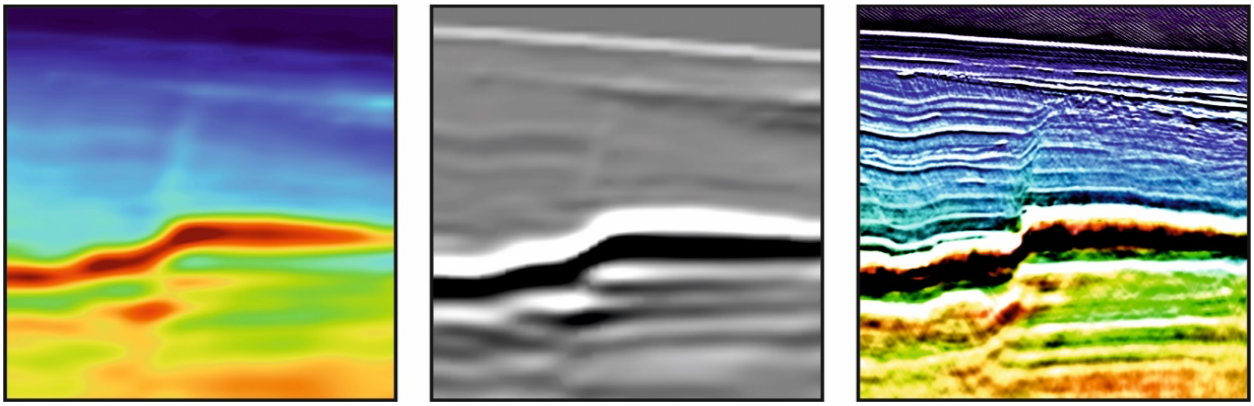

Figure 4: Detailed view of the top of the carbonate platform and its overlying sediments: AWI velocity (left) and reflectivity (center) models at 21.4 Hz, and (right) the corresponding Kirchhoff migration overlain on the AWI model. The steeply dipping feature in the models corresponds to the position of a steep fault and associated deformation zone.

seen in the 21.4 Hz model however are so clearly associated with such intense shear.

Conclusions

It can be useful to regard conventional FWI as a form of AWI with zero dimensions; conventional AWI as 1D AWI; the multi-channel version for streamer data as 2D AWI; and its analogue for ocean-bottom nodes under an array of regularly distributed sources as 3D AWI. Multi-dimensional AWI can deal with poor initial models and incomplete physics in the wavefield simulation during inversion, but practical applications using towed-streamer data are best utilized in combination with 1D AWI to ensure an exact final match to the kinematics of the field data without exaggerating fine detail in the model.

For acoustic inversion of datasets that show significant elastic effects, especially in the multiples, a final high-frequency pass of true-amplitude conventional FWI, over short offsets only, can also ensure that the true normal-incidence reflectivity is captured. For the moderately elastic marine dataset used here, 2D AWI was able to capture steep events in the velocity model that appear to relate to zones of enhanced simple shear; these were not captured by either 1D AWI or conventional FWI. The resulting AWI velocity model produced simpler structures in the Kirchhoff section, and significantly flatter gathers, than did a previous combination of reflection tomography and conventional FWI. We are currently repeating this inversion workflow elastically, which will allow a fully quantitative comparison of the derived acoustic and elastic models.

Acknowledgements

The authors would like to thank Woodside Energy (Egypt) Ltd for permission to present this work. The field-data example is shown with permission from TGS. Any views or opinions expressed in this paper are solely those of the authors and do not necessarily represent those of S-Cube or Woodside Energy.